CHAPTER 247
Undertow Profiles in the Bottom Boundary Layer under Breaking Waves

Daniel T. Cox[1] and Nobuhisa Kobayashi[2]

ABSTRACT: The vertical distribution of the mean shear stress inside the surf zone is compared to the terms in the time-averaged horizontal momentum equation using one set of laboratory measurements of the free surface elevations and fluid velocities u and w induced by regular waves spilling on a plane slope. The vertical distribution of the eddy viscosity is estimated directly from the measured mean shear stress and velocity. The shear stress distribution in the surf zone is shown to vary linearly with depth until the bottom boundary layer where it reached a nearly constant, negative value. The shear stress variation in the transition region differs distinctly from the inner surf zone. The vertical variation of $\overline{uw}$ is shown to be small outside the surf zone except near the bottom. Inside the surf zone, it is shown that the $\overline{uw}$ term of the horizontal momentum equation is likely to be important in the transition region and that its importance diminishes in the inner surf zone. The vertical distribution of the eddy viscosity has a form which is small near trough level, increases to a maximum value about one-third of the depth below trough level, and then decreases toward the bottom. The eddy viscosity in the middle of the bottom boundary layer is two orders of magnitude less than the eddy viscosity in the interior.

INTRODUCTION

Detailed cross-shore sediment transport models require accurate prediction of near-shore currents, particularly an accurate description of the flow in the bottom boundary layer under breaking waves. The horizontal component of the mean cross-shore flow, or undertow, is driven by the vertical imbalance of the depth-varying momentum flux and the depth-uniform pressure gradient due to the setup (Dyhr-Nielsen and Sørensen, 1970). In the last decade, several undertow models have been developed based on this concept and vary in the degree of empiricism, choice of boundary conditions, specification of eddy viscosity, and treatment of the bottom boundary layer (e.g., Dally and Dean, 1984; Svendsen, 1984; Stive and Wind, 1986; Svendsen *et al.*, 1987; Deigaard *et al.*, 1991; Stive and de Vriend, 1994). Cox *et al.* (1994) presented for the first time detailed laboratory measurements of the instantaneous velocities and shear stresses in the bottom boundary layer of about 1 cm thickness under breaking waves. In the present paper, these measurements are used to compare the vertical distribution of the mean shear stress to the terms of the time-averaged horizontal momentum equation and to estimate the vertical distribution of the eddy viscosity used to express the mean shear stress in terms of the mean horizontal velocity.

The time-averaged horizontal momentum equation may be written

$$\frac{\partial}{\partial z}\left(\frac{\overline{\tau}}{\rho}\right) = g\frac{\partial \overline{\eta}}{\partial x} + \frac{\partial}{\partial x}\left(\overline{u^2} - \overline{w^2}\right) + \frac{\partial \overline{uw}}{\partial z} = \alpha(x,z) \tag{1}$$

[1]Asst. Prof., Ocean Engrg. Prog., Dept. of Civil Engrg., Texas A&M Univ., College Station, TX 77843-3136, USA; Email: dtc@arlo.tamu.edu; Tel: +1 409 862 3627; Fax: +1 409 862 1542.

[2]Prof. and Assoc. Dir., Center for Applied Coastal Res., Univ. of Delaware, Newark, DE 19716, USA; Email: nk@coastal.udel.edu; Tel: +1 302 831 8044; Fax: +1 302 831 1228.

where x is the horizontal coordinate, positive onshore; z is the vertical coordinate, positive upward with $z = 0$ at the still water level (SWL); τ is the shear stress; ρ is the fluid density; η is the free surface elevation; u and w are the horizontal and vertical components of the fluid velocity; g is the gravitational acceleration; α is the vertical gradient of $\overline{\tau}/\rho$; and the overbar denotes time-averaging over the wave period. The subscripts x and z are used later to denote differentiation with respect to the horizontal and vertical coordinates. The mean shear stress $\overline{\tau}$ is generally related to the vertical gradient of the mean horizontal velocity $\overline{u}$ through an eddy viscosity ν_t in the following form:

$$\frac{\overline{\tau}}{\rho} = \nu_t \frac{\partial \overline{u}}{\partial z} \tag{2}$$

In this paper, each of the terms in (1) are analyzed using the laboratory measurements of Cox *et al.* (1994). The eddy viscosity is estimated using (2) with the measured values of $\overline{\tau}/\rho$ and $\overline{u}$.

The data of Cox *et al.* (1994) consists of free surface and velocity measurements for the case of regular waves spilling on a rough, impermeable 1:35 slope. The roughness consisted of a single layer of sand grains glued on the plane slope. The median diameter of the sand grains is $d_{50} = 0.10$ cm. The velocity profiles were measured at six vertical lines in the cross-shore direction to include the shoaling region seaward of breaking (denoted L1), the break point (L2), the transition region (L3) and the inner surf zone (L4, L5, and L6). Each of the measuring lines include measuring points at a fraction of the grain height above the rough, fixed bottom. Table 1 lists basic statistics of the data set where x is the cross-shore coordinate with $x = 0$ at L1 and $x = 980$ cm at the still water shoreline, H is the wave height, $\overline{h}$ is the local water depth including the setup, k is the wavenumber, η_{min} is the trough level, and $\overline{\eta}$ is the setup. The wave period is $T = 2.2$ s, and the free surface statistics are based on the phase-average of 50 waves.

Table 1: Measuring line locations and free surface statistics for L1 to L6.

Line.	x	H	$\overline{h}$	$k\overline{h}$	η_{min}	$\overline{\eta}$	$[\overline{\eta}_x]_m$	$[\overline{\eta}_x]_B$	Q_s
No.	(cm)	(cm)	(cm)		(cm)	(cm)	$\times 10^3$	$\times 10^3$	(cm^2/s)
L1	0	13.22	27.60	0.4982	-3.88	-0.30	-0.6	-0.5	-88
L2	240	17.10	20.64	0.4265	-3.60	-0.44	0.0	—	-99
L3	360	12.71	17.56	0.3917	-2.82	-0.05	3.3	4.6	-148
L4	480	8.24	14.38	0.3529	-2.33	0.20	3.3	3.1	-114
L5	600	7.08	11.51	0.3144	-1.60	0.75	3.3	3.3	-70
L6	720	5.05	8.50	0.2690	-0.82	1.13	3.3	3.5	-45

ANALYSIS OF HORIZONTAL MOMENTUM EQUATION

The shear stress appearing in (1) is estimated from the measurements assuming $\overline{\tau}/\rho = -\overline{\sigma_{uw}}$ where $\overline{\sigma_{uw}}$ is the time-average of the phase-averaged covariance of the measured horizontal and vertical velocity components (Cox *et al.*, 1995). Fig. 1 shows the vertical variation of $\overline{\tau}/\rho$ below trough level at the four measuring lines inside the surf zone. Outside the surf zone, $\overline{\tau}/\rho \simeq 0$ even in the bottom boundary layer (Cox *et al.*, 1995).

The mean water level and trough level corresponding to $\overline{\eta}$ and η_{min} of Table 1 are indicated in the figure with the long and short horizontal lines, respectively. The vertical variation of $\overline{\tau}/\rho$ below trough level increases from the transition region (L3) to the inner surf zone (L4). For the three measuring lines in the inner surf zone, the vertical variation of $\overline{\tau}/\rho$ is fairly linear and decreases with depth, as shown in Okayasu *et al.* (1988); but $\overline{\tau}/\rho$ is negative and almost constant in the bottom boundary layer. In the transition region, $\overline{\tau}/\rho$ also decreases linearly with depth, but the thickness for which $\overline{\tau}/\rho$ is negative is much larger.

The variations of $\overline{\tau}/\rho$ in the bottom boundary layer are shown in detail in the bottom panel of Fig. 1. A second vertical coordinate z_b is introduced and is related to the vertical coordinate z by $z = (z_b - d)$ where d is the depth below the SWL. This figure clearly shows that $\overline{\tau}/\rho$ is non-zero and negative near the bottom in the inner surf zone and could be modeled as depth-invariant near the bottom. The solid circle at $z_b = 0$ indicates $\overline{\tau}_b/\rho$ computed by a linear regression analysis assuming a logarithmic profile of the mean velocity in the bottom boundary layer (Cox and Kobayashi, 1996). The thick line indicates the 95% confidence interval from the regression analysis. These points are added as a check of the $\overline{\tau}/\rho$ estimates near the bottom. The temporal variations of the bottom shear stress τ_b were discussed in Cox *et al.* (1996).

The solid line in the upper and lower panels is a piecewise continuous line approximated by a constant shear stress in the bottom boundary layer and a linear best-fit line through the interior points. The constant shear stress was computed using a number of measured points, j, above the bottom as listed in Table 2. The number j was determined at each measuring line by choosing all of measured values for which $\overline{\tau}/\rho < 0$ near the bottom. The best-fit line through the interior points was estimated using the interior points from the jth point to the trough level. Because of the large scatter in $\overline{\tau}/\rho$ in the interior and because of a regression analysis minimizing the squared error, it was necessary to use a weighting function which emphasized the jth point by counting it ten times. The jth point is indicated in the figure with an open circle.

Table 2 lists the average shear stress in the bottom boundary layer, denoted $\overline{\tau}_b$. These values are reasonably close to the values obtained by Cox and Kobayashi (1996) as indicated in Fig. 1. Table 2 lists the vertical gradient of $\overline{\tau}/\rho$, denoted α, for the interior points using the weighted best-fit line. The uncertainty using a 95% confidence interval is indicated in parenthesis. The value of α without the weighting, denoted α_*, is also indicated in Table 2 with the 95% confidence interval. The values of α and α_* are similar, and the effect of the weighting is to change the intercept of the best-fit line rather than its slope. The confidence intervals, however, were affected since the weighting function effectively doubled the number of points in the regression analysis; hence, the uncertainties based on the unweighted regression analysis are adopted hereafter as realistic estimates. For completeness, Table 2 lists an estimate of the boundary layer thickness δ defined here as the location where the shear stress changes sign from negative to positive. The boundary layer thickness is approximately $\delta \simeq 0.9$ cm in the inner surf zone, similar to the values obtained by Cox *et al.* (1996). At L3, the shear stress changes sign at a much higher elevation, $\delta \simeq 5$ cm, which may not give a good indication of the actual boundary layer thickness in the transition region.

The setup gradient $\overline{\eta}_x$ is the dominant term on the right-hand-side of (1) in the surf

Table 2: Shear stress estimates and gradients for L3 to L6.

Line. No.	j	$\overline{\tau}_b/\rho$ (cm^2/s^2)	α (cm/s^2)	α_* (cm/s^2)	δ (cm)
L3	14	-1.1	1.1 (0.2)	1.1 (0.6)	4.5
L4	10	-0.8	2.6 (0.5)	2.3 (1.0)	1.0
L5	9	-0.5	1.9 (0.3)	1.7 (0.5)	0.7
L6	8	-0.6	2.8 (0.3)	2.6 (0.5)	0.8

zone. The estimates of $\overline{\eta}_x$ are listed in Table 1, where the m subscript is used to denote the gradient estimated from the measured $\overline{\eta}$. For L1, $\overline{\eta}_x$ is estimated by a forward difference of the measured values at L1 and L2. For L2, no estimate is given, although $\overline{\eta}_x \simeq 0$ at the break point (e.g., Bowen *et al.*, 1968). For L3 to L6, $\overline{\eta}_x$ is estimated using a linear regression which includes an additional measuring value of $\overline{\eta} = 1.45$ cm at $x = 840$ cm (Cox *et al.*, 1995). The regression analysis indicated

$$\overline{\eta}_x = (3.3 \pm 0.6) \times 10^{-3}, \quad \gamma_{xy}^2 = 0.988$$

where the uncertainty is estimated by a 95% confidence interval and γ_{xy}^2 is the square of the correlation coefficient. To check the accuracy of $\overline{\eta}_x$ estimated from the measurements, comparisons were made with $\overline{\eta}_x$ estimated using the analytical expression in Bowen *et al.* (1968). These analytical values are listed in Table 1 and are indicated with the B subscript. The agreement is good except at L3 where the analytical $\overline{\eta}_x$ may be overpredicted.

The second term on the right-hand-side of (1) involves the horizontal and vertical velocities, u and w, which can be expressed as the sum of the orbital velocity, denoted with a tilde, and the mean velocity, denoted with an overbar,

$$u = \tilde{u} + \overline{u} \quad \text{and} \quad w = \tilde{w} + \overline{w} \tag{3}$$

The time-average of the squared velocities may be written

$$\overline{u^2} = \overline{\tilde{u}^2} + \overline{u}^2 \quad \text{and} \quad \overline{w^2} = \overline{\tilde{w}^2} + \overline{w}^2 \tag{4}$$

Undertow models based on (1) generally assume that $u \simeq \tilde{u}$ and $w \simeq \tilde{w}$. As a further simplification, it is often assumed that $\overline{u^2}$ is depth-invariant and that $\overline{w^2}/\overline{u^2} << 1$. Fig. 2 shows the vertical variation of $\overline{u^2}$, $\overline{u}^2$, and $\overline{w^2}$ for L1 to L6. This figure indicates that $\overline{u^2}$ is nearly constant over depth, except very near the bottom and that $\overline{w^2}/\overline{u^2} << 1$ is a reasonable assumption, except near the trough level. Outside the surf zone, the approximation of $u \simeq \tilde{u}$ is also quite good since $\overline{u}^2 \simeq 0$ everywhere below trough level. Inside the surf zone, however, the magnitude of $\overline{u}^2$ is sufficiently large compared to $\overline{u^2}$. Table 3 lists the depth-averaged values of $\overline{u^2}$, $\overline{\tilde{u}^2}$, and $\overline{u}^2$ where the a subscript denotes averaging from the trough level to the bottom. Outside the surf zone, $[\overline{u}^2]_a/[\overline{u^2}]_a \simeq 0.05$, and inside the surf zone, $[\overline{u}^2]_a/[\overline{u^2}]_a \simeq 0.25$. Table 3 also indicates that the vertical velocity component is negligible both outside and inside the surf zone, $[\overline{w^2}]_a/[\overline{u^2}]_a \simeq 0.05$, except near trough level where $[\overline{w^2}]_{tr}/[\overline{u^2}]_{tr} \simeq 0.15$.

Table 3: Depth-averaged values and horizontal gradients of $\overline{u^2}$, $\overline{\tilde{u}^2}$, and $\overline{u}^2$ for L1 to L6.

Line No.	$\left[\overline{u^2}\right]_a$ (cm/s)^2	$\left[\overline{\tilde{u}^2}\right]_a$ (cm/s)^2	$\left[\overline{u}^2\right]_a$ (cm/s)^2	$\frac{\partial}{\partial x}\left[\overline{u^2}\right]_a$ (cm/s^2)	$\frac{\partial}{\partial x}\left[\overline{\tilde{u}^2}\right]_a$ (cm/s^2)	$\frac{\partial}{\partial x}\left[\overline{u}^2\right]_a$ (cm/s^2)	$\frac{\left[\overline{w^2}\right]_a}{\left[\overline{u^2}\right]_a}$	$\frac{\left[\overline{w^2}\right]_{tr}}{\left[\overline{u^2}\right]_{tr}}$
L1	473	460	13	0.09	0.01	0.07	0.080	0.20
L2	494	464	30	-0.4	-0.9	0.4	0.071	0.19
L3	410	307	103	-0.8	-1.0	0.2	0.054	0.16
L4	309	220	89	-0.5	-0.4	-0.2	0.036	0.11
L5	260	202	58	-0.5	-0.4	-0.2	0.031	0.09
L6	183	135	48	-0.5	-0.4	-0.2	0.022	0.07

Fig. 3 shows the cross-shore variation of the depth-averaged values of $\overline{u^2}$, $\overline{\tilde{u}^2}$, and $\overline{u}^2$ with the horizontal gradients. The estimates of the horizontal gradients are listed in Table 3. At L1, L2 and L3, the gradients were computed using finite differences as follows: L1, forward difference with $(\mathrm{L2}-\mathrm{L1})/(\Delta x)$ with $\Delta x = 240$ cm from Table 1; L2, central difference with $(-\mathrm{L1}-3\mathrm{L2}+4\mathrm{L3})/(6\Delta x)$ with $\Delta x = 120$ cm; and L3, central difference with $(\mathrm{L4}-\mathrm{L2})/(2\Delta x)$ with $\Delta x = 120$ cm. The horizontal step size is large given that the vertical resolution of the measuring points is only a few centimeters in the interior and a few millimeters near the bottom. The gradients for L4, L5 and L6 were computed using linear regression which gave

$$(\overline{u^2})_x = -0.5 \pm 0.3 \text{ cm/s}^2, \quad \gamma^2_{xy} = 0.98$$
$$(\overline{\tilde{u}^2})_x = -0.4 \pm 0.5 \text{ cm/s}^2, \quad \gamma^2_{xy} = 0.90$$
$$(\overline{u}^2)_x = -0.2 \pm 0.2 \text{ cm/s}^2, \quad \gamma^2_{xy} = 0.93$$

Although there is large uncertainty in the horizontal gradient estimates, the analysis based on the depth-averaged values of $\overline{u^2}$, $\overline{\tilde{u}^2}$, and $\overline{u}^2$ indicates that the approximation of $u \simeq \tilde{u}$ is reasonable for estimating the horizontal gradient of the $\overline{u^2}$ term in (1) in the surf zone.

Deigaard and Fredsøe (1989) indicated the importance of $\overline{uw}$ appearing in the third term on the right-hand-side of (1). Fig. 4 shows the temporal variation of uw with u and w at five elevations $z = -7.9$, -15.9, -23.9, -26.9, and -27.8 cm, indicated (a) to (e), respectively, for L1. In this figure, uw is reduced by a factor of 10 to facilitate plotting, and the phases have been adjusted such that the zero upcrossing of the free surface elevation is at $t = T/4 = 0.55$ s. The figure shows that the variation in uw is large, especially in the upper portion of the water column $z = -7.9$ cm (a) where uw reaches a maximum value of $uw \simeq 500$ cm^2/s^2. Near the bottom at $z = -27.8$ cm (e), uw is small since the vertical velocity component is approximately zero.

Fig. 5 shows the vertical variation of the time-averaged value of uw below trough level for L1 to L6. The time-averaged values for the five elevations in Fig. 4 are indicated by a solid circle for L1. The magnitude of $\overline{uw}$ is 10 cm^2/s^2 which is an order of

magnitude less than the fluctuations of uw shown in Fig. 4. Outside the surf zone, $\overline{uw}$ is nearly depth-invariant except near the bottom. Inside the surf zone, the variation of $\overline{uw}$ is noisy. Nevertheless, crude estimates of the vertical gradients of the $\overline{uw}$ at L3 and L4 may be made. At L3, $(\overline{uw})_z \sim (-2.7)$ cm/s^2 in the lower portion of the water column, and $(\overline{uw})_z \sim 2.3$ cm/s^2 in the upper portion. These estimates were made "by eye" using the curves of Fig. 5 re-plotted on a separate sheet of graph paper. The uncertainties are roughly ±50%. For L4, $(\overline{uw})_z \sim (-2.5)$ cm/s^2 in the lower portion of the water column. In the upper portion, $(\overline{uw})_z$ is approximately zero. For L5 and L6, $(\overline{uw})_z$ is small. Again, these are very crude estimates based on time-averaged quantities that are an order of magnitude less than the fluctuating quantities.

Considering (3), the $\overline{uw}$ term can be expressed as

$$\overline{uw} = \overline{\tilde{u}\tilde{w}} + (\overline{u}\,\overline{w}) \tag{5}$$

and the assumption of a weak current gives $\overline{uw} \simeq \overline{\tilde{u}\tilde{w}}$. Fig. 5 indicates that the $(\overline{u}\,\overline{w})$ term is indeed small below trough level and in the bottom boundary layer outside the surf zone. Inside the surf zone, the $(\overline{u}\,\overline{w})$ term appears to give a substantial contribution to the $\overline{uw}$ term.

Table 4 summarizes the quantification of the terms in the horizontal momentum equation (1) based on the measurements of Cox *et al.* (1994) inside the surf zone. The uncertainties are indicated in parenthesis. The table indicates that for L4 and L6 in the inner surf zone, the shear stress gradient is balanced by the sum of the first two terms on the right-hand-side of (1). The relative error is less than 5% for both L4 and L6 which is well within the uncertainty of the estimates. For L5, the measured shear stress gradient is smaller than for L4 and L6, but the gradient is still balanced by the first two terms within the uncertainties of the measurements. At L3 however, the measured shear stress gradient is smaller than the sum of the first two term by a factor of two. Therefore, it is likely that the $\overline{uw}$ term plays an important role in the transition region and that its importance decreases in the inner surf zone. Outside the surf zone, the gradient of $\overline{uw}$ is small, except in the bottom boundary layer.

Table 4: Summary of terms in horizontal momentum equation for L3 to L6.

Line. No.	$(\overline{\tau}/\rho)_z$ (cm/s^2)	$g\,\overline{\eta}_x$ (cm/s^2)	$\left(\left[\overline{u^2}\right]_a\right)_x$ (cm/s^2)	$(\overline{uw})_z$ (cm/s^2)
L3	1.1 (0.6)	3.2 (0.6)	-0.8 (0.5)	-2.7 to 2.3
L4	2.6 (1.0)	3.2 (0.6)	-0.5 (0.3)	-2.5 to 0
L5	1.9 (0.5)	3.2 (0.6)	-0.5 (0.3)	small
L6	2.8 (0.5)	3.2 (0.6)	-0.5 (0.3)	small

ESTIMATE OF EDDY VISCOSITY

The use of (2) in undertow models requires the specification of an eddy viscosity, ν_t. Several forms have been proposed including depth-invariant, two-layer, parabolic, and piecewise continuous. The eddy viscosity is specified empirically, with a velocity scale related to the wave celerity or to the local turbulent kinetic energy and a length scale related to the local water depth.

In this paper, ν_t is estimated from (2) using the measured values of $\overline{\tau}/\rho$ and $\overline{u}$. The left panel of Fig. 6 shows the vertical variation of the measured $\overline{u}$ with a best-fit cubic spline at L4. The values of the seaward volume flux, Q_s, per unit width listed in Table 1 were calculated by integrating this curve from the bottom where $\overline{u} = 0$ to just above trough level where again $\overline{u} = 0$. The middle panel of Fig. 6 shows the measured values of $\overline{\tau}/\rho$ below trough level and is the same as that plotted at L4 in Fig. 1. The right panel shows the eddy viscosity at L4 estimated from

$$\nu_t = \frac{\overline{\tau}/\rho}{(\overline{u})_z} \tag{6}$$

where $\overline{\tau}/\rho$ is given by the piecewise continuous best fit curve and the vertical gradient of the horizontal velocity is estimated from the best-fit cubic spline using a finite difference approximation with a vertical resolution of $\Delta z = 0.01$ cm. The figure shows that from trough level, the eddy viscosity increases downward to a maximum value about one-third of the depth below trough level and then decreases. The variation in the eddy viscosity is unrealisticly large as the velocity gradient approaches zero at $z \simeq (-12)$ cm. This is the major limitation of the eddy viscosity approach. Near the bottom, the eddy viscosity is small as the velocity gradient becomes large.

Fig. 7 shows the vertical variation of the measured eddy viscosity at the four measuring lines inside the surf zone similar to the right panel of Fig 6. Only those portions for which (6) gave reasonable estimates are shown. The vertical distribution of the eddy viscosity is qualitatively similar for L4, L5, and L6 in the inner surf zone. For L3, reasonable estimates could not be obtained over most of the depth. The magnitude of ν_t in the bottom boundary layer for the four measuring lines is

$$\nu_t = 0.10 \pm 0.05 \text{ cm}^2/\text{s} \quad \text{at} \quad z_b = 0.5 \text{ cm}$$

and is about two order of magnitude smaller than ν_t estimated in the interior. This large decrease is consistent with the assumption made by Svendsen *et al.* (1987).

CONCLUSIONS

The following conclusions are supported in this paper based on the analysis of one set of laboratory measurements of regular wave spilling on a rough, plane slope.

- The mean shear stress distribution in the inner surf zone varies linearly with depth until the bottom boundary layer where it reaches a nearly constant, negative value. The bottom shear stress is also negative. The shear stress variation in the transition region differs distinctly from the inner surf zone in that the negative shear stress extends much higher in the water column.

- The $\overline{w^2}$ term is negligible compared to $\overline{u^2}$ except near the trough level.
- Outside the surf zone, $\overline{u}^2/\overline{u^2} << 1$. Inside the surf zone, $\overline{u}^2$ contributes significantly to $\overline{u^2}$. The approximation of $u \simeq \tilde{u}$, however, is reasonable for estimating the horizontal gradient of $\overline{u^2}$ inside the surf zone.
- The vertical variation of $\overline{uw}$ is small outside the surf zone except near the bottom.
- The shear stress gradient can be balanced by the first two terms of the horizontal momentum equation (1) in the inner surf zone.
- The $\overline{uw}$ term is likely to be important in the transition region and its importance diminishes in the inner surf zone.
- The vertical distribution of the eddy viscosity in the surf zone estimated from the measured mean shear stress and horizontal velocity has a form which is small near trough level, increases to a maximum value about one-third of the depth below trough level, and then decreases toward the bottom.
- The eddy viscosity in the middle of the bottom boundary layer is two orders of magnitude less that the eddy viscosity in the interior.

Dynamic undertow models based on (1) and (2) are difficult to apply with confidence because of the many uncertainties involved in estimating the terms in (1) and the eddy viscosity in (2). An alternative kinematic model is proposed by Cox and Kobayashi (1996). This model relates the horizontal velocity, bottom shear stress, and boundary layer thickness in a simple but general manner.

ACKNOWLEDGMENTS

This work was sponsored by the U.S. Army Research Office, University Research Initiative under contract No. DAAL03-92-G-0116 and by the National Science Foundation under grant No. CTS-9407827.

REFERENCES

Bowen, A., Inman, D., and Simmons, V. (1968) "Wave 'set-down' and setup." *J. Geophys. Res.*, 73, 2569–2577.

Cox, D.T. and Kobayashi, N. (1996) "A kinematic undertow model with a logarithmic boundary layer." *J. Waterway, Port, Coastal, and Ocean Engrg.*, (submitted).

Cox, D. T., Kobayashi, N., and Okayasu, A. (1994) "Vertical variations of fluid velocities and shear stress in surf zones." *Proc. 24th Coast. Engrg. Conf.*, ASCE, 1, 98–112.

Cox, D.T., Kobayashi, N., and Okayasu, A. (1995) "Experimental and numerical modeling of surf zone hydrodynamics." *Rpt. No. CACR-95-07*, Center for Applied Coastal Research, University of Delaware, Newark, Delaware, 293 p.

Cox, D.T., Kobayashi, N., and Okayasu, A. (1996). "Bottom shear stress in the surf zone." *J. Geophys. Res.*, 111 (C6), 14337–14348.

Dally, W.B. and Dean, R.G. (1984). "Suspended sediment transport and beach evolution." *J. Waterway, Port, Coastal, and Ocean Engrg.*, 110 (1), 15–33.

Deigaard R. and Fredsøe, J. (1989). "Shear stress distribution in dissipative water waves." *Coast. Engrg.*, 13, 357–378.

Deigaard, R., Justesen, P., and Fredsøe, J. (1991). "Modeling of undertow by a one-equation turbulence model." *Coast. Engrg.*, 15, 431–458.

Dyhr-Nielsen, M. and Sørensen, T. (1970). "Sand transport phenomena on coasts with bars." *Proc. 12th Coast. Engrg. Conf.*, ASCE, 182–192.

Okayasu, A., Shibayama, T., and Horikawa, K. (1988) "Vertical variation of undertow in the surf zone." *Proc. 21rd Coast. Engrg. Conf.*, ASCE, 478–491.

Stive, M. J. F. and de Vriend, H. J. (1994) "Shear stresses and mean flow in shoaling and breaking waves." *Proc. 24th Coast. Engrg. Conf.*, ASCE, 1, 594–608.

Stive, M.J.F. and Wind, H.G. (1986) "Cross-shore mean flow in the surf zone." *Coast. Engrg.*, 10, 325–340.

Svendsen, I. A. (1984) "Mass flux and undertow in a surf zone." *Coast. Engrg.*, 8, 247-365.

Svendsen, I. A., Schäffer, H. A., and Hansen J. B. (1987) "The interaction between the undertow and the boundary layer flow on a beach." *J. Geophys. Res.*, 92(C11), 11845–11856.

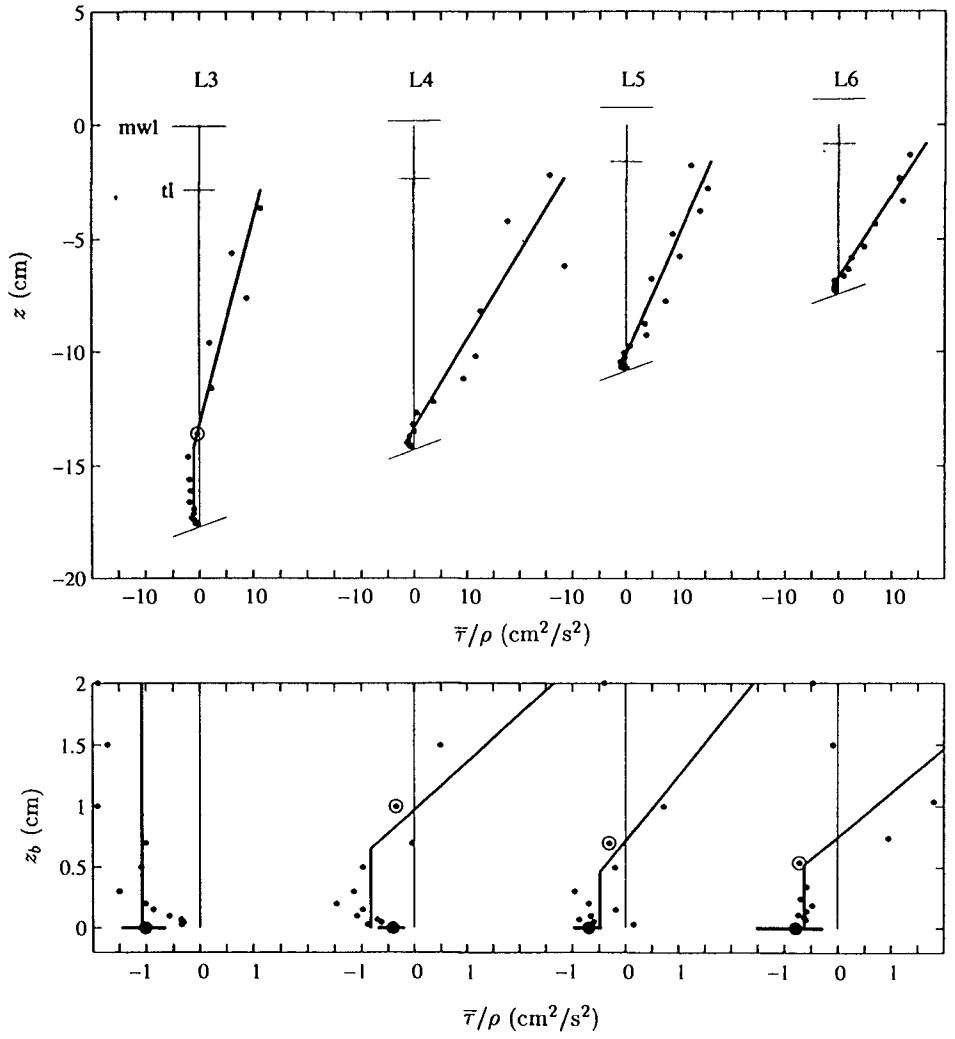

Figure 1: Vertical variation of measured shear stress $\overline{\tau}/\rho$ (•) with piecewise continuous best-fit line (——) (top) and detail in bottom boundary layer with $\overline{\tau}_b$ from linear regression (●) and 95% confidence interval (——) for L3 to L6. Circle indicates jth elevation listed in Table 2.

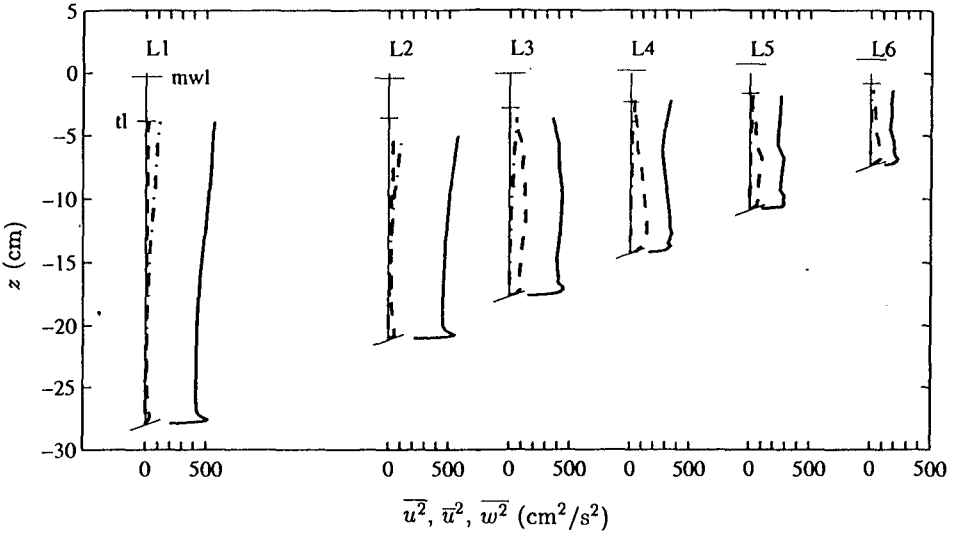

Figure 2: Vertical variation of $\overline{u^2}$ (——), $\overline{u}^2$ (– –), and $\overline{w^2}$ (–·–) for L1–L6.

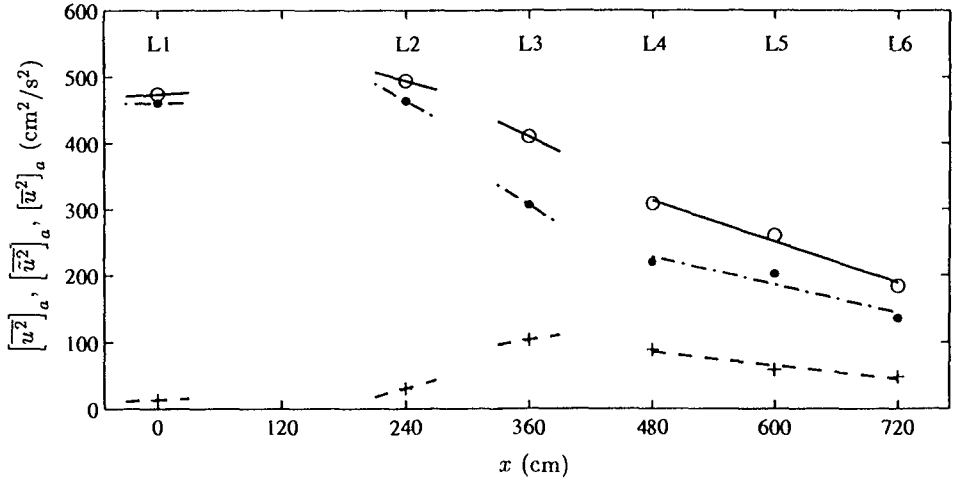

Figure 3: Cross-shore variation of $\left[\overline{u^2}\right]_a$ (○ ——), $\left[\overline{\tilde{u}^2}\right]_a$ (• –·–), and $\left[\overline{u}^2\right]_a$ (+ – –) with gradients for L1–L6.

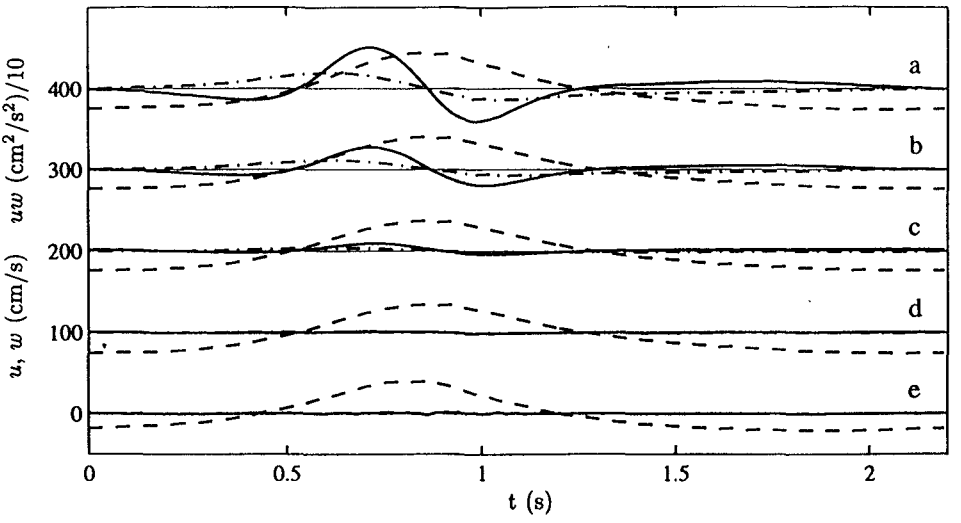

Figure 4: Temporal variation of u (– –), w (–·–), and uw (——) at five elevations for L1. To facilitate plotting, uw is reduced by a factor of 10, and there is an offset of a factor of 100 in the ordinate.

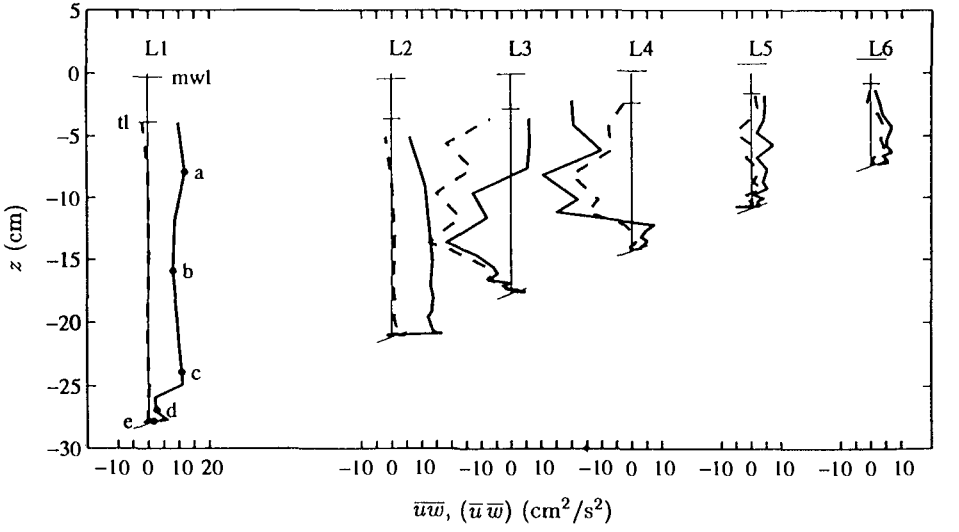

Figure 5: Vertical variation of $\overline{uw}$ (——) and $(\overline{u}\,\overline{w})$ (– –), for L1–L6. Five elevations of Fig. 4 at L1 indicated by solid circle (•).

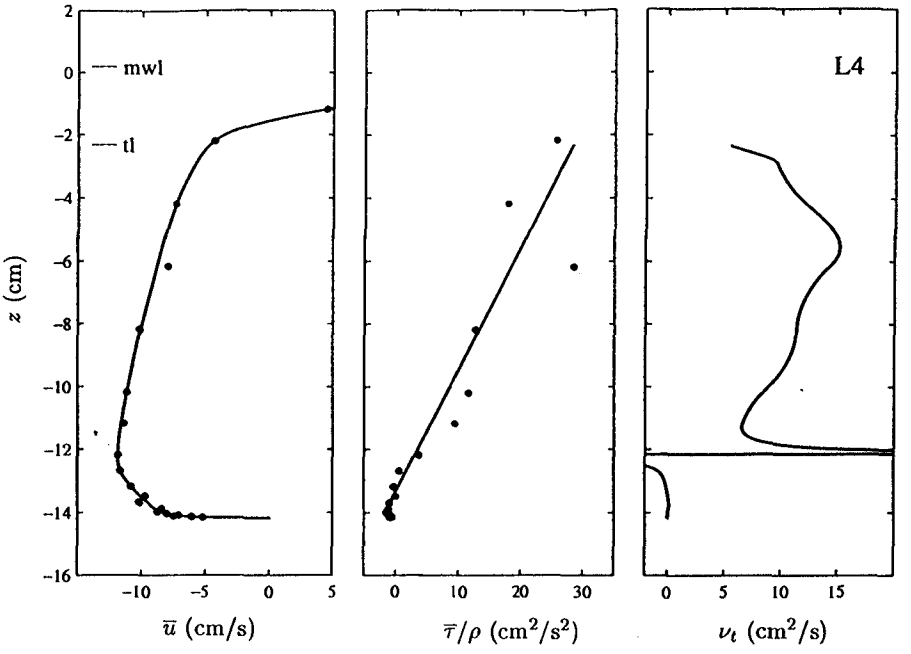

Figure 6: Vertical variation of measured $\overline{u}$ (•) with cubic spline (——) (left); measured shear stress $\overline{\tau}/\rho$ (•) with best-fit curve (——) (middle); kinematic viscosity ν_t (——) (right) for L4.

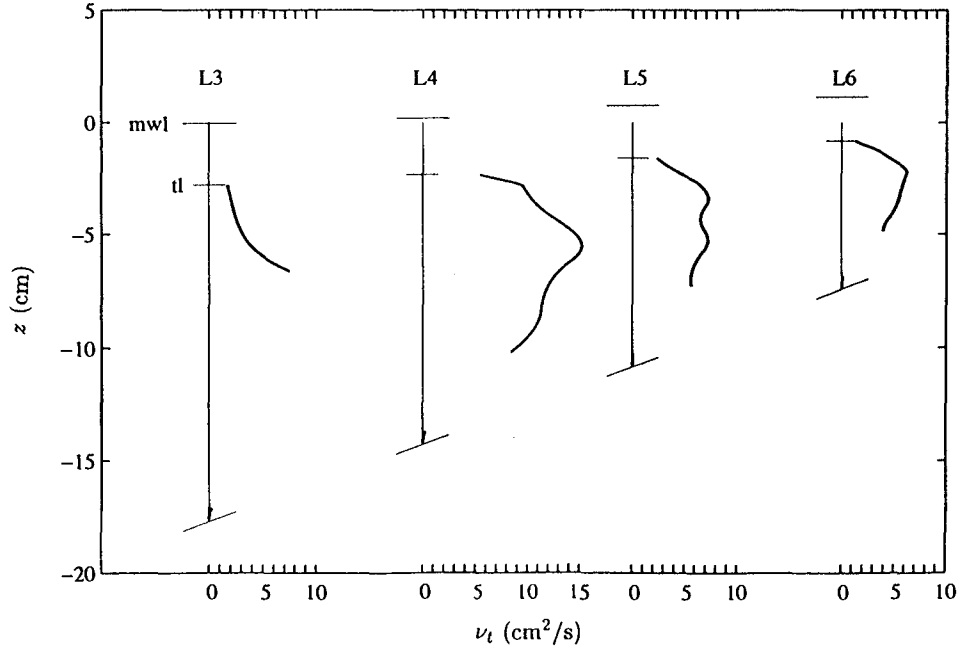

Figure 7: Vertical variation of measured eddy viscosity ν_t (——) for L3 to L6.